Characterization of Nonlinear Behavior of Weakly Coupled Resonators Based on Nonlinearity Factor

Tamio Ikehashi, *Member, IEEE*, Hideyuki Maekoba, and Arnaud Parent

***Abstract*—Mode-localization is a promising method to realize high sensitivity sensors, especially in the field of MEMS. Since these sensors monitor amplitude change of weakly coupled resonators, it is important to grasp condition that induces multi-valued amplitude-frequency curve. In this paper, we provide an efficient tool to characterize the nonlinear behavior of the weakly coupled resonators. To analyze the nonlinearity, we solve a two-degrees-of-freedom (2-DoF) coupled equation of motion with nonlinear spring terms. Two approximations are employed to solve the equation; Krylov–Bogoliubov averaging method and approximation based on eigenmode amplitude-ratio at the resonances. As a result, we obtain two decoupled Duffing-like amplitude-frequency equations. We show that nonlinearity of the system is described by factors contained in the equations. The factors can be explicitly written in terms of basic parameters of the system, including coupling spring constant and nonlinear terms. Thus, instead of relying on numerical calculations, we can find parameter condition that brings about multi-valued amplitude-frequency curve. This method can also be utilized to find a condition that eliminates the nonlinearity. As an example, we apply this method to a weakly coupled resonator which uses parallel plate electrode as a coupling spring. We demonstrate the effectiveness and validity of this method by comparing the result with FEM simulations. The methodology and results presented here are general one and can be applied to various systems described by nonlinear coupled resonators.**

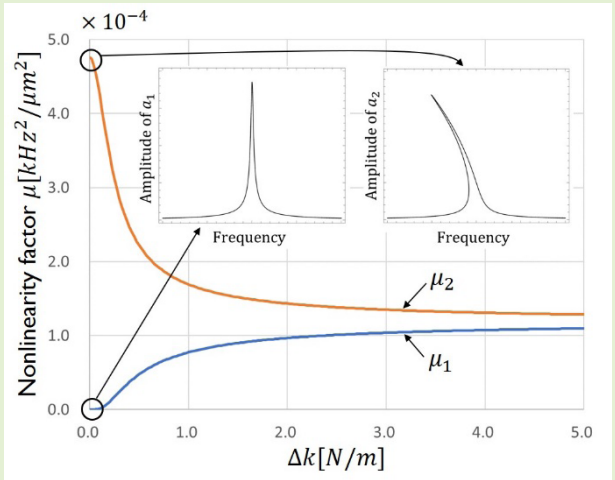

***Index Terms*— Duffing resonator, MEMS, mode-localization, nonlinear, weakly coupled resonator.**

I. Introduction

SENSORS using mode localization, or mode-localized sensors, have been extensively studied to realize various high sensitivity MEMS sensors [1]–[4]. The high sensitivity is originating from large amplitude change of weakly coupled resonators (WCRs). The amplitude change is brought by small perturbation of mass or spring stiffness that constitute the WCR. This kind of amplitude-based sensing method is shown to have higher sensitivity compared to frequency-based sensing methods [5], [6]. To date, various types of sensors are proposed based on this method, including mass sensors [1], accelerometers [7]–[9], charge sensors [10], and magnetometers [11].

In mode-localized sensors, large signal-to-noise ratio (SNR) can be attained for large amplitudes. However, if the amplitude becomes too large, Duffing-like nonlinearity will emerge in the amplitude-frequency property. In this case, due to the hysteresis of multi-valued amplitude-frequency curve, the peak amplitude condition cannot be sustained by a naive closed-loop system that does not use phase information. In this sense, nonlinearity affects dynamic range of the sensor and also architecture of the sensor system. The nonlinearity is caused by spring hardening or by nonlinear electrostatic force used for the coupling spring. Recently, nonlinearity of mode-localized sensors is investigated from several perspectives. One work proposes to cancel the mechanical nonlinearity by optimizing the electrostatic force [12]. Another work tries to eliminate a nonlinearity originating from electrostatic force by introducing shaped combs [13]. On the other hand, utilization of nonlinear regime is proposed to enhance the SNR, with the use of closed-loop phase feedback [14]–[16].

To design mode-localized sensor system and to explore possibilities of using nonlinear regime, it is crucial to grasp a

Manuscript received August 10, 2021; revised September 8, 2021; accepted September 20, 2021. Date of publication September 22, 2021; date of current version October 29, 2021. The associate editor coordinating the review of this article and approving it for publication was Dr. Yong Zhu. *(Corresponding author: Tamio Ikehashi.)*

Tamio Ikehashi is with the Graduate School of Information Production and Systems, Waseda University, Fukuoka 808-0135, Japan (e-mail: t.ikehashi@waseda.jp).

Hideyuki Maekoba and Arnaud Parent are with Coventor, A Lam Research Company, Yokohama 222-0033, Japan (e-mail: hideyuki.maekoba@lamresearch.com; aparent@coventor.com).

Digital Object Identifier 10.1109/JSEN.2021.3114992

condition of parameters that brings about nonlinearity. However, an obstacle in analyzing the nonlinearity of WCRs is that the equation of motion cannot be solved analytically. This is due to the coupled and nonlinear nature of the equation of motion. The theoretical analysis to date therefore needs to rely on simulations. It is, however, difficult to grasp the behavior of whole parameter space from such case-by-case simulations. This paper tries to provide a useful tool for this kind of nonlinear analysis. Especially, according to the method provided in this paper, parameter condition that induces multi-valuedness in the amplitude-frequency curve can be found without solving the nonlinear equation.

To analyze the WCR equation, we first employ Krylov–Bogoliubov averaging method [17], [18]. This is a well-known method to find approximate solutions of Duffing-like nonlinear equations. However, since our equations are coupled, this alone will not lead to useful results. Recently, Yang et al have applied this method to solve an equation identical to WCR, but their result was not simple enough, and need to rely on numerical calculation to demonstrate the result [19]. In view of this, we introduce another approximation based on eigenmode amplitude ratio at the resonance. We apply this method to a general form of nonlinear 2-DoF WCR. Namely, nonlinearity is introduced up to fourth order for the three springs, i.e., two springs that support the masses and one coupling spring. Damping terms are also introduced in the equation. Furthermore, we consider a case of two independent external driving forces. Thus, our method can be applied to the case of double-resonators drive method [7]. If the two approximations are applied to this system, we arrive at two decoupled Duffing-like amplitude-frequency equations corresponding to the two modes. Nonlinearity and coupling effect of the resonator are reflected in "nonlinearity factors" contained in the decoupled equation. We show that nonlinear behavior is represented by these nonlinearity factors, which are explicitly written in terms of basic parameters of the system. Especially, we can find combination of parameters that can cancel the nonlinearity. Finally, the validity of the result is verified by comparing the theoretical model with FEM simulations.

This paper is organized as follows: In section II, we review essence of mode-localized sensors and WCR for the linear case. Then, in section III, we try to derive an approximate solution of nonlinear WCR. Nonlinearity factors will be introduced here. Some asymptotic expressions of the nonlinearity factors are presented, and their meaning are discussed. Finally, in section IV, we examine a case which employs parallel plate electrode as the coupling spring. Numerical comparison with FEM simulations are carried out in this example. Conclusion of the paper will be given at the end.

II. Review of Linear Mode-Localized Sensors

We first review the essence of linear mode-localized sensors. Formulation presented here will also be utilized in the nonlinear case. Especially, we point out that approximation based on eigenmode amplitude ratio, which is playing a key role in the nonlinear case, is also used in the linear case.

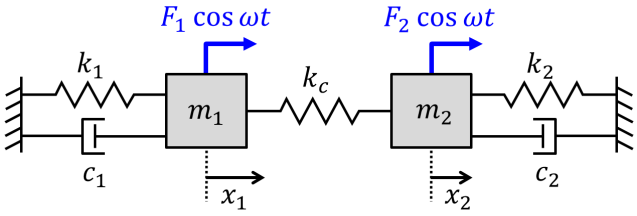

Fig. 1. Schematic of coupled resonator system.

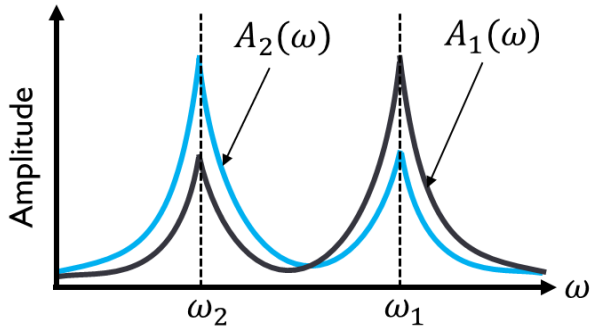

Fig. 2. Amplitude A_1 and A_2 as a function of angular frequency ω. Due to the coupling spring, both amplitudes have two resonances corresponding to ω_1 and ω_2.

A. Brief Summary of Mode-Localized Sensors

We consider a coupled resonator shown in Fig. 1. The system consists of masses $m_i (i = 1, 2)$, damping coefficients c_i, spring constants k_i and k_c. Position of the mass m_i is denoted as x_i. All springs are linear in this case. When an external force $F_i \cos \omega t$ is applied to each mass m_i, equation of motion becomes

$$m_1 \ddot{x}_1 + c_1 \dot{x}_1 + k_1 x_1 + k_c (x_1 - x_2) = F_1 \cos \omega t, \quad (1)$$

$$m_2 \ddot{x}_2 + c_2 \dot{x}_2 + k_2 x_2 - k_c (x_1 - x_2) = F_2 \cos \omega t. \quad (2)$$

A stationary state solution of this coupled equation can be written in a form

$$\begin{pmatrix} x_1 \\ x_2 \end{pmatrix} = \begin{pmatrix} A_1 \cos(\omega t + \Phi_1) \\ A_2 \cos(\omega t + \Phi_2) \end{pmatrix}, \quad (3)$$

where A_i is amplitude and Φ_i is phase. These factors are function of the angular frequency ω. Since this is 2-DoF system, it possesses two resonances ω_1 and ω_2 corresponding to the two eigen modes. Due to the coupling k_c, both A_1 and A_2 have two resonances, as illustrated in Fig. 2.

In mode-localized sensors, ratio of the amplitudes at the resonance, $u_1 = A_2(\omega_1)/A_1(\omega_1)$ or $u_2 = A_2(\omega_2)/A_1(\omega_2)$ are measured. Let's now suppose that we initially have conditions $k_1 = k_2 \equiv k$ and $m_1 = m_2 \equiv m$. Then we consider a case when the spring constant k_1 has changed as $k \to k + \Delta k$ due to a physical perturbation. For example, in the case of accelerometer, Δk is caused by an acceleration [7], [8]. We write the initial amplitude ratio as u_1^0, u_2^0 and amplitude

ratio after the perturbation as u_1, u_2. Then when $\Delta k \ll k_c$, they are shown to become $u_1^0 = -1$, $u_2^0 = +1$ and

$$u_1 \approx -1 + \frac{\Delta k}{2k_c}, \tag{4}$$

$$u_2 \approx +1 + \frac{\Delta k}{2k_c}. \tag{5}$$

Therefore if we define sensitivities by $S_1 = \left|(u_1 - u_1^0)/u_1^0\right|$ and $S_2 = \left|(u_2 - u_2^0)/u_2^0\right|$, they are expressed as

$$S_1 = S_2 = \left|\frac{\Delta k}{2k_c}\right|. \tag{6}$$

This result suggests higher sensitivity can be attained for smaller k_c.

The shift $k \to k + \Delta k$ can also be derived by monitoring the resonance frequency shift Δf. Sensing method based on this frequency-shift is also widely used [5]. In this case, the sensitivity $\Delta f/f$ caused by Δk is $\left|\Delta k/(2k)\right|$. This suggests that the sensitivity of mode-localized sensor is higher than that of the frequency-shift based approach by a factor of $\left|k/k_c\right|$ [2], [3].

B. Derivation of Sensitivity for Linear Case

Extension of the linear approach to nonlinear case will require detailed knowledge on the linear formulation, which is essentially an eigenvalue problem of coupled resonators. Here, we summarize essential points of the linear formulation.

In the following, we assume $c_1/m_1 = c_2/m_2 \equiv b$. Then the coupled equation can be rewritten as

$$\begin{pmatrix} \ddot{x}_1 \\ \ddot{x}_2 \end{pmatrix} + b \begin{pmatrix} \dot{x}_1 \\ \dot{x}_2 \end{pmatrix} + K \begin{pmatrix} x_1 \\ x_2 \end{pmatrix} = \begin{pmatrix} f_1 \\ f_2 \end{pmatrix} \cos \omega t, \tag{7}$$

where $f_1 \equiv F_1/m_1$, $f_2 \equiv F_2/m_2$ and

$$K \equiv \begin{pmatrix} \dfrac{k_1 + k_c}{m_1} & -\dfrac{k_c}{m_1} \\ -\dfrac{k_c}{m_2} & \dfrac{k_2 + k_c}{m_2} \end{pmatrix}. \tag{8}$$

The matrix K can be diagonalized with a matrix P and can be expressed as

$$P^{-1} K P = \begin{pmatrix} \omega_1^2 & 0 \\ 0 & \omega_2^2 \end{pmatrix}. \tag{9}$$

If we introduce

$$\begin{pmatrix} z_1 \\ z_2 \end{pmatrix} \equiv P^{-1} \begin{pmatrix} x_1 \\ x_2 \end{pmatrix}, \tag{10}$$

$$\begin{pmatrix} \tilde{f}_1 \\ \tilde{f}_2 \end{pmatrix} \equiv P^{-1} \begin{pmatrix} f_1 \\ f_2 \end{pmatrix}, \tag{11}$$

the equations for z_i will become decoupled;

$$\begin{pmatrix} \ddot{z}_1 \\ \ddot{z}_2 \end{pmatrix} + b \begin{pmatrix} \dot{z}_1 \\ \dot{z}_2 \end{pmatrix} + \begin{pmatrix} \omega_1^2 & 0 \\ 0 & \omega_2^2 \end{pmatrix} \begin{pmatrix} z_1 \\ z_2 \end{pmatrix} = \begin{pmatrix} \tilde{f}_1 \\ \tilde{f}_2 \end{pmatrix} \cos \omega t. \tag{12}$$

The stationary state solution of this equation has a form

$$\begin{pmatrix} z_1 \\ z_2 \end{pmatrix} = \begin{pmatrix} a_1 \cos(\omega t + \phi_1) \\ a_2 \cos(\omega t + \phi_2) \end{pmatrix}, \tag{13}$$

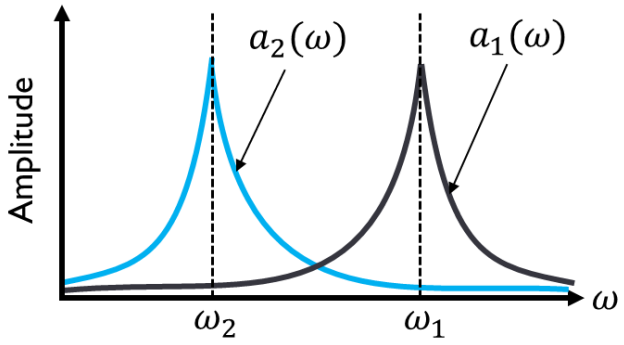

Fig. 3. Eigenmode amplitudes a_1 and a_2 as a function of ω. Since a_i is amplitude of eigenmode, it has single peak at ω_i. This leads to $a_1(\omega_1) \gg a_2(\omega_1)$ and $a_2(\omega_2) \gg a_1(\omega_2)$.

where

$$a_i = \frac{\tilde{f}_i}{\sqrt{\left(\omega_i^2 - \omega^2\right)^2 + (b\omega)^2}}, \tag{14}$$

$$\phi_i = \tan^{-1}\left[\frac{b\omega}{\omega^2 - \omega_i^2}\right]. \tag{15}$$

Here, z_i's are eigenmodes. We would like to call their amplitude a_i as eigenmode amplitude. Multiplying P from the left to (13), we can obtain x_1 and x_2. If matrix element of P is denoted as p_{ij}, then explicit form of A_i and Φ_i are obtained as

$$A_1 = \sqrt{p_{11}^2 a_1^2 + p_{12}^2 a_2^2 + 2p_{11}p_{12}a_1a_2\cos(\phi_1 - \phi_2)}, \tag{16}$$

$$A_2 = \sqrt{p_{21}^2 a_1^2 + p_{22}^2 a_2^2 + 2p_{21}p_{22}a_1a_2\cos(\phi_1 - \phi_2)}, \tag{17}$$

$$\Phi_1 = -tan^{-1}\left[\frac{p_{11}a_1\sin\phi_1 + p_{12}a_2\sin\phi_2}{p_{11}a_1\cos\phi_1 + p_{12}a_2\cos\phi_2}\right], \tag{18}$$

$$\Phi_2 = -\tan^{-1}\left[\frac{p_{21}a_1\sin\phi_1 + p_{22}a_2\sin\phi_2}{p_{21}a_1\cos\phi_1 + p_{22}a_2\cos\phi_2}\right]. \tag{19}$$

Since z_i's are eigenmodes, eigenmode amplitude a_i has single peak at resonant angular frequency ω_i, as illustrated in Fig. 3. Therefore at ω_1, $a_1(\omega_1) \gg a_2(\omega_1)$ holds. This suggests that we can make an approximation based on eigenmode amplitude ratio at ω_1;

$$A_1(\omega_1) = p_{11}a_1\left[1 + \mathrm{O}\left(\frac{a_2}{a_1}\right)\right] \approx p_{11}a_1, \tag{20}$$

$$A_2(\omega_1) = p_{21}a_1\left[1 + \mathrm{O}\left(\frac{a_2}{a_1}\right)\right] \approx p_{21}a_1. \tag{21}$$

Here, $\mathrm{O}\left(a_2/a_1\right)$ means that the term is at most proportional the small quantity a_2/a_1. Thus for the present case, it can be neglected compared to the first term. Similarly, at ω_2, $a_2(\omega_2) \gg a_1(\omega_2)$ holds. We therefore get

$$A_1(\omega_2) = p_{12}a_2\left[1 + \mathrm{O}\left(\frac{a_1}{a_2}\right)\right] \approx p_{12}a_2, \tag{22}$$

$$A_2(\omega_2) = p_{22}a_2\left[1 + \mathrm{O}\left(\frac{a_1}{a_2}\right)\right] \approx p_{22}a_2. \tag{23}$$

Thus u_1 and u_2, i.e., amplitude ratios at ω_1 and ω_2, can be approximated as

$$u_1 = \frac{A_2(\omega_1)}{A_1(\omega_1)} \approx \frac{p_{21}}{p_{11}}, \tag{24}$$

$$u_2 = \frac{A_2(\omega_2)}{A_1(\omega_2)} \approx \frac{p_{22}}{p_{12}}. \tag{25}$$

Note that the eigenmode amplitudes a_i's are cancelled out and the result just becomes ratio of the matrix elements. This property is retained even for the nonlinear case. Also, it turns out that the approximations based on eigenmode amplitude ratio at the resonance can also be used in the nonlinear analysis, as we will see later. This approximation is especially effective in high quality factor resonators.

Now let's assume that $k_1 = k + \Delta k$, $k_2 = k$, and $m_1 = m_2 \equiv m$. In this case, the amplitude ratio becomes

$$u_1 = \frac{\Delta k - \sqrt{\Delta k^2 + 4k_c^2}}{2k_c}, \tag{26}$$

$$u_2 = \frac{\Delta k + \sqrt{\Delta k^2 + 4k_c^2}}{2k_c}. \tag{27}$$

If we further assume $\Delta k \ll k_c$, we obtain the results of (4), (5), and the sensitivity (6).

In WCRs, quite small value is used for the coupling spring constant k_c. It is thus tempting to consider the case of $k_c \ll \Delta k$. In this case, if we assume $\Delta k > 0$ and use $\sqrt{\Delta k^2 + 4k_c^2} \approx \Delta k + 2k_c^2/\Delta k$, we get following results by neglecting higher order terms of $k_c/\Delta k$;

$$u_1 \approx -\frac{k_c}{\Delta k}, \tag{28}$$

$$u_2 \approx \frac{\Delta k}{k_c}. \tag{29}$$

Thus, in the limit of $k_c \ll \Delta k$, $u_1 \to 0$ and $u_2 \to \infty$. Initial states corresponding to $\Delta k = 0$ are the same as before, namely, $u_1^0 = -1$, $u_2^0 = +1$. Hence, sensitivities for this case become

$$S_1 = \left| \frac{u_1 - u_1^0}{u_1^0} \right| \approx 1, \tag{30}$$

$$S_2 = \left| \frac{u_2 - u_2^0}{u_2^0} \right| \approx \left| \frac{\Delta k}{k_c} \right|. \tag{31}$$

This suggests that when $k_c \ll \Delta k$, high sensitivity is attained only in the second mode S_2.

III. Nonlinear Weakly Coupled Resonators

We next consider a case when nonlinearity exists for the three springs k_1, k_2 and k_c. To solve the equations, we employ two approximations; Krylov–Bogoliubov averaging method, and approximation based on eigenmode amplitude ratio at the resonance.

A. Equation of Motion With Nonlinear Springs

In the equation of motion, we introduce nonlinearity up to fourth order in the displacements. On the other hand, to get analytical results, we assume $m_1 = m_2 \equiv m$ and $c_1 = c_2 \equiv c$. Then the equation of motion can be written as

$$\begin{aligned} m\ddot{x}_1 &+ c\dot{x}_1 + k_{11}x_1 + k_{12}x_1^2 + k_{13}x_1^3 + k_{14}x_1^4 \\ &+ k_{c1}(x_1 - x_2) + k_{c2}(x_1 - x_2)^2 + k_{c3}(x_1 - x_2)^3 \\ &+ k_{c4}(x_1 - x_2)^4 = F_1 \cos\omega t, \end{aligned} \tag{32}$$

$$\begin{aligned} m\ddot{x}_2 &+ c\dot{x}_2 + k_{21}x_2 + k_{22}x_2^2 + k_{23}x_2^3 + k_{24}x_2^4 \\ &- k_{c1}(x_1 - x_2) - k_{c2}(x_1 - x_2)^2 - k_{c3}(x_1 - x_2)^3 \\ &- k_{c4}(x_1 - x_2)^4 = F_2 \cos\omega t. \end{aligned} \tag{33}$$

Note that k_1, k_2, and k_c of (1) and (2) are replaced by k_{11}, k_{21}, and k_{c1}, respectively. Using a matrix representation as in the linear case, the equations can be rewritten as

$$\begin{aligned} \begin{pmatrix} \ddot{x}_1 \\ \ddot{x}_2 \end{pmatrix} + b\begin{pmatrix} \dot{x}_1 \\ \dot{x}_2 \end{pmatrix} + K\begin{pmatrix} x_1 \\ x_2 \end{pmatrix} + \begin{pmatrix} g_c \\ -g_c \end{pmatrix} + \begin{pmatrix} g_1 \\ g_2 \end{pmatrix} \\ = \begin{pmatrix} f_1 \\ f_2 \end{pmatrix} \cos\omega t, \end{aligned} \tag{34}$$

where $b \equiv c/m$, $f_i \equiv F_i/m$,

$$K \equiv \begin{pmatrix} \dfrac{k_{11} + k_{c1}}{m} & -\dfrac{k_{c1}}{m} \\ -\dfrac{k_{c1}}{m} & \dfrac{k_{21} + k_{c1}}{m} \end{pmatrix}, \tag{35}$$

and g_c, g_1, and g_2 represent contributions from nonlinear terms,

$$g_c \equiv \epsilon_{c2}(x_1 - x_2)^2 + \epsilon_{c3}(x_1 - x_2)^3 + \epsilon_{c4}(x_1 - x_2)^4, \tag{36}$$

$$g_1 \equiv \epsilon_{12}x_1^2 + \epsilon_{13}x_1^3 + \epsilon_{14}x_1^4, \tag{37}$$

$$g_2 \equiv \epsilon_{22}x_2^2 + \epsilon_{23}x_2^3 + \epsilon_{24}x_2^4 \tag{38}$$

with ϵ_{cn} and $\epsilon_{in} (n = 2, 3, 4)$ defined by

$$\epsilon_{cn} \equiv \frac{k_{cn}}{m}, \epsilon_{in} \equiv \frac{k_{in}}{m}. \tag{39}$$

Applying diagonalization to (34), we obtain

$$\begin{aligned} \begin{pmatrix} \ddot{z}_1 \\ \ddot{z}_2 \end{pmatrix} + b\begin{pmatrix} \dot{z}_1 \\ \dot{z}_2 \end{pmatrix} + \begin{pmatrix} \omega_1^2 & 0 \\ 0 & \omega_2^2 \end{pmatrix}\begin{pmatrix} z_1 \\ z_2 \end{pmatrix} + P^{-1}\begin{pmatrix} g_c \\ -g_c \end{pmatrix} + \begin{pmatrix} \tilde{g}_1 \\ \tilde{g}_2 \end{pmatrix} \\ = \begin{pmatrix} \tilde{f}_1 \\ \tilde{f}_2 \end{pmatrix} \cos\omega t, \end{aligned} \tag{40}$$

where

$$\begin{pmatrix} \tilde{g}_1 \\ \tilde{g}_2 \end{pmatrix} \equiv P^{-1}\begin{pmatrix} g_1 \\ g_2 \end{pmatrix}. \tag{41}$$

Explicit forms of the matrix P and the resonant angular frequencies ω_1 and ω_2 are given in Appendix.

B. Krylov–Bogoliubov Averaging Method

To solve the nonlinear equation, we first employ Krylov–Bogoliubov averaging method [17], [18]. This is a method to obtain an approximate solution of first order nonlinear differential equation

$$\dot{X} = \varepsilon f(t), \tag{42}$$

where X is a time dependent variable, ε is a small parameter, and $f(t)$ is a periodic function. If the period is T, $f(t)$ satisfies $f(t + T) = f(t)$. This function $f(t)$ can be nonlinear. If the

change in a period is small enough, $f(t)$ may be replaced with the averaged value over the period. Namely, the differential equation can be approximated as

$$\dot{X} = \varepsilon \langle f \rangle, \tag{43}$$

where $\langle f \rangle$ is an average of $f(t)$ over the period T;

$$\langle f \rangle = \frac{1}{T} \int_0^T dt f(t). \tag{44}$$

This approximation is shown to be valid up to $O(\varepsilon)$, which means that the difference between $f(t)$ and $\langle f \rangle$ is at most proportional to the small quantity ε. This is the core idea of the averaging method. Practically, we often need to recast the equation to the form of (42) so that this method can be applied. The averaging method is shown to be useful for nonlinear oscillating system such as Duffing oscillator [18].

Now let's apply the averaging method to (34). Firstly, we need to rewrite the equation into a form of first order differential equation. To this end, we introduce parameters y_1, y_2 and recast (34) into state space representation,

$$\begin{pmatrix} \dot{x}_1 \\ \dot{x}_2 \end{pmatrix} = \begin{pmatrix} y_1 \\ y_2 \end{pmatrix}, \tag{45}$$

$$\begin{pmatrix} \dot{y}_1 \\ \dot{y}_2 \end{pmatrix} = -b \begin{pmatrix} y_1 \\ y_2 \end{pmatrix} - K \begin{pmatrix} x_1 \\ x_2 \end{pmatrix} - \begin{pmatrix} g_c \\ -g_c \end{pmatrix} - \begin{pmatrix} g_1 \\ g_2 \end{pmatrix} + \begin{pmatrix} f_1 \\ f_2 \end{pmatrix} \cos \omega t. \tag{46}$$

Here, we regard that parameters b, f_i, ϵ_{cn}, and ϵ_{in} are all small and $O(\varepsilon)$. The $O(\varepsilon^0)$ solution, namely, the solution when these parameters are zero, are given by

$$\begin{pmatrix} x_1 \\ x_2 \end{pmatrix} = P \begin{pmatrix} a_1 \cos(\omega t + \phi_1) \\ a_2 \cos(\omega t + \phi_2) \end{pmatrix}, \tag{47}$$

$$\begin{pmatrix} y_1 \\ y_2 \end{pmatrix} = P \begin{pmatrix} -a_1 \omega \sin(\omega t + \phi_1) \\ -a_2 \omega \sin(\omega t + \phi_2) \end{pmatrix}, \tag{48}$$

where a_i and ϕ_i are time independent constants. To find the solution for non-zero parameters b, f_i, ϵ_{cn}, and ϵ_{in}, we employ a method of variation of constants. Namely, we regard that a_i and ϕ_i are now time dependent parameters; $a_i(t)$, $\phi_i(t)$. Also, we denote $\omega t + \phi_i(t) \equiv \theta_i$. Then from (45), (46) and recalling the diagonalized expression (40), we obtain equations for $a_i(t)$ and $\phi_i(t)$ as

$$\begin{pmatrix} \dot{a}_1 \cos\theta_1 - a_1 \dot{\phi}_1 \sin\theta_1 \\ \dot{a}_2 \cos\theta_2 - a_2 \dot{\phi}_2 \sin\theta_2 \end{pmatrix} = \begin{pmatrix} 0 \\ 0 \end{pmatrix}, \tag{49}$$

$$\begin{pmatrix} \dot{a}_1 \sin\theta_1 + a_1 \dot{\phi}_1 \cos\theta_1 \\ \dot{a}_2 \sin\theta_2 + a_2 \dot{\phi}_2 \cos\theta_2 \end{pmatrix} = -b \begin{pmatrix} a_1 \sin\theta_1 \\ a_2 \sin\theta_2 \end{pmatrix} - \frac{1}{\omega} \left\{ \begin{pmatrix} (\omega^2 - \omega_1^2) a_1 \cos\theta_1 \\ (\omega^2 - \omega_2^2) a_2 \cos\theta_2 \end{pmatrix} + \begin{pmatrix} \sigma_1 \\ \sigma_2 \end{pmatrix} g_c - \begin{pmatrix} \tilde{g}_1 \\ \tilde{g}_2 \end{pmatrix} + \begin{pmatrix} \tilde{f}_1 \\ \tilde{f}_2 \end{pmatrix} \cos \omega t \right\}, \tag{50}$$

where

$$\begin{pmatrix} \sigma_1 \\ \sigma_2 \end{pmatrix} \equiv P^{-1} \begin{pmatrix} -1 \\ 1 \end{pmatrix}. \tag{51}$$

These equations can be solved with respect to $a_i(t)$ and $\phi_i(t)$. The result becomes

$$\dot{a}_1 = \sin\theta_1 \left[-b a_1 \sin\theta_1 - \frac{\omega^2 - \omega_1^2}{\omega} a_1 \cos\theta_1 - \frac{1}{\omega} \left(\sigma_1 g_c - \tilde{g}_1 + \tilde{f}_1 \cos \omega t \right) \right], \tag{52}$$

$$\dot{\phi}_1 = \cos\theta_1 \left[-b \sin\theta_1 - \frac{\omega^2 - \omega_1^2}{\omega} \cos\theta_1 - \frac{1}{\omega a_1} \left(\sigma_1 g_c - \tilde{g}_1 + \tilde{f}_1 \cos \omega t \right) \right], \tag{53}$$

$$\dot{a}_2 = \sin\theta_2 \left[-b a_2 \sin\theta_2 - \frac{\omega^2 - \omega_2^2}{\omega} a_2 \cos\theta_2 - \frac{1}{\omega} \left(\sigma_2 g_c - \tilde{g}_2 + \tilde{f}_2 \cos \omega t \right) \right], \tag{54}$$

$$\dot{\phi}_2 = \cos\theta_2 \left[-b \sin\theta_2 - \frac{\omega^2 - \omega_2^2}{\omega} \cos\theta_2 - \frac{1}{\omega a_2} \left(\sigma_2 g_c - \tilde{g}_2 + \tilde{f}_2 \cos \omega t \right) \right]. \tag{55}$$

Up to here, no approximation is made. To apply the averaging method, we assume $\omega^2 - \omega_1^2 \sim O(\varepsilon)$ and $\omega^2 - \omega_2^2 \sim O(\varepsilon)$. This means that for (52) and (53), we are trying to find a behavior at the vicinity of ω_1. Similarly, for (54) and (55), we are thinking the behavior at the vicinity of ω_2. Then, all the terms in r.h.s. of (52) to (55) becomes $O(\varepsilon)$. Thus, we are now able to apply the averaging method. Let's first apply the averaging method to (52). The equation then becomes

$$\dot{a}_1 = -b a_1 \left\langle \sin^2\theta_1 \right\rangle - \frac{\omega^2 - \omega_1^2}{\omega} a_1 \langle \cos\theta_1 \sin\theta_1 \rangle - \frac{1}{\omega} \langle \sigma_1 g_c \sin\theta_1 - \tilde{g}_1 \sin\theta_1 \rangle - \frac{\tilde{f}_1}{\omega} \langle \sin\theta_1 \cos \omega t \rangle. \tag{56}$$

Here, the bracket $\langle \cdot \rangle$ means time averaging over a period of $2\pi/\omega$. Recalling that $\theta_1 = \omega t + \phi_1$, we find $\left\langle \sin^2\theta_1 \right\rangle = 1/2$, $\langle \cos\theta_1 \sin\theta_1 \rangle = 0$, and

$$\langle \sin\theta_1 \cos \omega t \rangle = \frac{\omega}{2\pi} \int_0^{2\pi/\omega} dt \sin(\omega t + \phi_1) \cos \omega t = \frac{1}{2} \sin\phi_1. \tag{57}$$

Thus the equation reduces to

$$\dot{a}_1 = -\frac{b}{2} a_1 - \frac{1}{\omega} \langle \sigma_1 g_c \sin\theta_1 - \tilde{g}_1 \sin\theta_1 \rangle - \frac{\tilde{f}_1}{2\omega} \sin\phi_1. \tag{58}$$

The remaining bracket $\langle \sigma_1 g_c \sin\theta_1 - \tilde{g}_1 \sin\theta_1 \rangle$ can be calculated explicitly, but since it becomes lengthy, we just cast them in Appendix. Similarly, we can apply avaraging to (53)-(55) and the results become

$$\dot{\phi}_1 = -\frac{\omega^2 - \omega_1^2}{2\omega} - \frac{1}{\omega a_1} \langle \sigma_1 g_c \cos\theta_1 - \tilde{g}_1 \cos\theta_1 \rangle - \frac{\tilde{f}_1}{2\omega a_1} \cos\phi_1, \tag{59}$$

$$\dot{a}_2 = -\frac{b}{2}a_2 - \frac{1}{\omega}\langle\sigma_2 g_c \sin\theta_2 - \tilde{g}_2 \sin\theta_2\rangle - \frac{\tilde{f}_2}{2\omega}\sin\phi_2, \quad (60)$$

$$\dot{\phi}_2 = -\frac{\omega^2-\omega_2^2}{2\omega} - \frac{1}{\omega a_2}\langle\sigma_2 g_c \cos\theta_2 - \tilde{g}_2 \cos\theta_2\rangle - \frac{\tilde{f}_2}{2\omega a_2}\cos\phi_2. \quad (61)$$

Explicit forms of remaining bracket terms are also shown in the Appendix. It should be noticed that as a result of the averaging, terms originating from x_i^2 and x_i^4 in the equation of motion (32) and (33) have disappeared. This is because these terms are symmetric with respect to $x_i = 0$ and thus became zero after the averaging. Thus the third power term x_i^3 is now the only nolinear contribution.

C. Approximation Based on Eigenmode Amplitude Ratio

The results after the averaging, (58)-(61), are still complicated and cannot be solved analytically. But here, we can see that the brackets in (58)-(61) are expressed by terms proportional to a_1^3, $a_1^2 a_2$, $a_1 a_2^2$ and a_2^3. Therefore, approximation based on eigenmode amplitude ratio at the resonance can be applied. Note that a_1 and a_2 are eigenmode amplitudes that have single peak as indicated in Fig. 3, and they are different from physically observable amplitudes A_1 and A_2 shown in Fig. 2.

Firstly, at $\omega \sim \omega_1$, $a_1(\omega_1) \gg a_2(\omega_1)$ holds. Thus, the brackets in (58) and (59) are expressed as

$$\langle\sigma_1 g_c \sin\theta_1 - \tilde{g}_1 \sin\theta_1\rangle = a_1^3 \cdot \mathrm{O}\left(\frac{a_2}{a_1}\right), \quad (62)$$

$$\langle\sigma_1 g_c \cos\theta_1 - \tilde{g}_1 \cos\theta_1\rangle = \frac{1}{2}\mu_1 a_1^3\left[1 + \mathrm{O}\left(\frac{a_2}{a_1}\right)\right], \quad (63)$$

where

$$\mu_1 \equiv \frac{3}{4}\left\{\epsilon_{c3}\sigma_1\rho_1^3 - \epsilon_{13}\left(p^{-1}\right)_{11}(p_{11})^3 - \epsilon_{23}\left(p^{-1}\right)_{12}(p_{21})^3\right\}, \quad (64)$$

$$\begin{pmatrix}\rho_1\\ \rho_2\end{pmatrix} \equiv P^T\begin{pmatrix}1\\ -1\end{pmatrix} = \begin{pmatrix}p_{11}-p_{21}\\ p_{12}-p_{22}\end{pmatrix}, \quad (65)$$

and $\left(p^{-1}\right)_{ij}$ are matrix elements of P^{-1} and P^T is transpose of P. We call the factor μ_1 as a nonlinearity factor.

Secondly, at $\omega \sim \omega_2$, we have $a_2(\omega_2) \gg a_1(\omega_2)$. In this case, the brackets in (60) and (61) are expressed as

$$\langle\sigma_2 g_c \sin\theta_2 - \tilde{g}_2 \sin\theta_2\rangle = a_2^3 \cdot \mathrm{O}\left(\frac{a_1}{a_2}\right), \quad (66)$$

$$\langle\sigma_2 g_c \cos\theta_2 - \tilde{g}_2 \cos\theta_2\rangle = \frac{1}{2}\mu_2 a_2^3\left[1 + \mathrm{O}\left(\frac{a_1}{a_2}\right)\right], \quad (67)$$

where

$$\mu_2 \equiv \frac{3}{4}\left\{\epsilon_{c3}\sigma_2\rho_2^3 - \epsilon_{13}\left(p^{-1}\right)_{21}(p_{12})^3 - \epsilon_{23}\left(p^{-1}\right)_{22}(p_{22})^3\right\}. \quad (68)$$

The factor μ_2 is a nonlinearity factor corresponding to the second mode. If we only retain lowest order terms of the eigenmode amplitude ratio, (58)-(61) reduces to

$$\dot{a}_1 = -\frac{b}{2}a_1 - \frac{\tilde{f}_1}{2\omega}\sin\phi_1, \quad (69)$$

$$\dot{\phi}_1 = -\frac{\omega^2-\omega_1^2}{2\omega} - \frac{\mu_1}{2\omega}a_1^2 - \frac{\tilde{f}_1}{2\omega a_1}\cos\phi_1, \quad (70)$$

$$\dot{a}_2 = -\frac{b}{2}a_2 - \frac{\tilde{f}_2}{2\omega}\sin\phi_2, \quad (71)$$

$$\dot{\phi}_2 = -\frac{\omega^2-\omega_2^2}{2\omega} - \frac{\mu_2}{2\omega}a_2^2 - \frac{\tilde{f}_2}{2\omega a_2}\cos\phi_2. \quad (72)$$

This is the result of the second approximation. Note that the first mode equations (69), (70) and the second mode equations (71), (72) are now seemingly decoupled. Actually, the coupling effect due to the coupling spring k_{c1} still exists in the form of matrix element p_{ij} and $(p^{-1})_{ij}$ in the nonlinearity factors μ_1 and μ_2.

D. Amplitude-Frequency Equation for Stationary State

Stationary state solutions of (69)-(72) are obtained by setting $\dot{a}_i = 0$ and $\dot{\phi}_i = 0$, which means that a_i and ϕ_i are constants. If we eliminate ϕ_i, we get equations for the eigenmode amplitudes a_i;

$$\left[b^2\omega^2 + \left(\omega^2 - \omega_1^2 + \mu_1 a_1^2\right)^2\right]a_1^2 = \tilde{f}_1^2, \quad (73)$$

$$\left[b^2\omega^2 + \left(\omega^2 - \omega_2^2 + \mu_2 a_2^2\right)^2\right]a_2^2 = \tilde{f}_2^2. \quad (74)$$

We thus arrived at two Duffing type amplitude-frequency equations corresponding to the two modes. We can now see that the nonlinearity factors μ_1 and μ_2 represent nonlinear effect originating from the third power terms ϵ_{c3}, ϵ_{13}, and ϵ_{23}. We can also confirm that the linear expression (14) can be reproduced when the nonlinearity factors are zero; $\mu_i = 0$. Positive and negative nonlinearity factors correspond to spring hardening and softening, respectively. The expression of μ_i shows that they can be positive or negative, depending on parameters ϵ_{c3}, ϵ_{13}, ϵ_{23} and the matrix P. This also implies possibility of eliminating the nonlinearity by optimizing the parameters of μ_i. This is already demonstrated for a specific case [12]. The explicit form of the nonlinearity factors, (64) and (68), enables to clarify the cancellation condition in general form.

We can also derive the expressions for the phase ϕ_i. They also become Duffing type;

$$\phi_1 = \tan^{-1}\left[\frac{b\omega}{\omega^2 - \omega_1^2 + \mu_1 a_1^2}\right], \quad (75)$$

$$\phi_2 = \tan^{-1}\left[\frac{b\omega}{\omega^2 - \omega_2^2 + \mu_2 a_2^2}\right]. \quad (76)$$

As before, the linear result (15) can be regained in the limit $\mu_i \to 0$.

E. Critical Point of Nonlinearity

In this section, we derive a critical point that defines border of single-valued and multi-valued amplitude-frequency curves. Let's consider amplitude-frequency curve described by

$$\left[b^2\omega^2 + \left(\omega^2 - \omega_i^2 + \mu_i a_i^2\right)^2\right]a_i^2 = \tilde{f}_i^2. \quad (77)$$

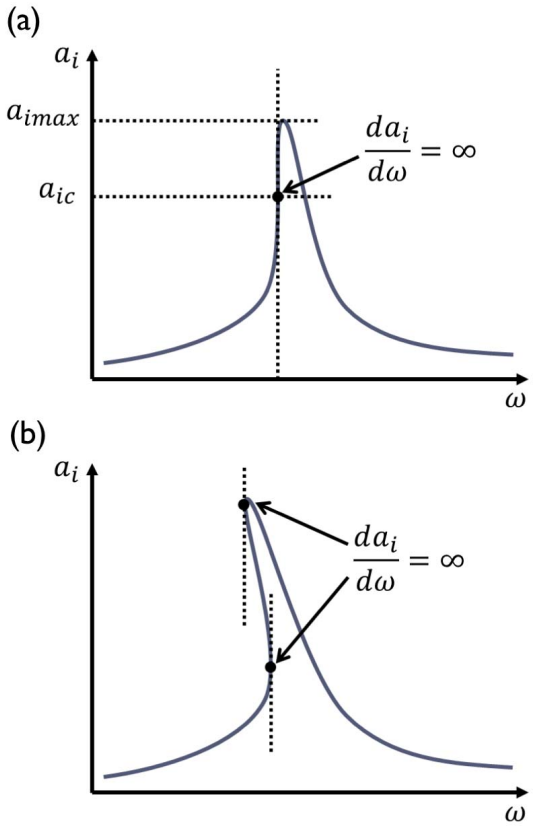

Fig. 4. (a) Amplitude-frequency curve of critical condition which has single bifurcation point that satisfies $da_i/d\omega = \infty$. Eigenmode amplitude is a single-valued function. (b) Amplitude-frequency curve of double bifurcation point case. Eigenmode amplitude is a multi-valued function.

We assume that μ_i is non-zero. If the force $\tilde{f}_i$ is small enough, the eigenmode amplitude will become a single-valued function of the frequency. If $\tilde{f}_i$ is increased, the amplitude-frequency curve will exhibit a single bifurcation point represented by the infinite slope condition $da_i/d\omega = \infty$, as shown in Fig. 4 (a). In this state, the amplitude-frequency curve is still a single valued function. But if $\tilde{f}_i$ is increased further, multiple bifurcation point will appear as in Fig. 4 (b). This suggests that the eigenmode amplitude is now a multi-valued function of the frequency. It also implies emergence of hysteresis in the amplitude-frequency plot.

Let's find the critical condition of Fig. 4 (a). This corresponds to a case which has only one solution satisfying $da_i/dw = \infty$ [20], [21]. Solving this, we obtain the critical eigenmode amplitude

$$a_{ic} = \sqrt{\frac{b\omega_i}{|\mu_i|}}\left[1 - \frac{b^2}{4\omega_i^2}\right]^{\frac{1}{4}} \approx \sqrt{\frac{b\omega_i}{|\mu_i|}}, \tag{78}$$

where we assumed $b \ll \omega_i$ in the last step, which is justified for large quality factor. From (77) and (78), we can get the critical force as

$$\tilde{f}_{ic} = \sqrt{\frac{2b^3\omega_i^3}{|\mu_i|}}. \tag{79}$$

We can also derive the peak eigenmode amplitude;

$$a_{imax} \approx \sqrt{\frac{2b\omega_i}{|\mu_i|}} = \sqrt{2}a_{ic}. \tag{80}$$

Note that similar arguments hold for fixed force $\tilde{f}_i$ and variable nonlinearity factor. Namely, if $|\mu_i|$ is increased for fixed $\tilde{f}_i$, the double bifurcation occurs when

$$|\mu_i| > \frac{2b^3\omega_i^3}{\tilde{f}_i^2} \tag{81}$$

is satisfied. Thus, together with explicit form of the nonlinearity factor μ_i, we can find the condition that brings about multi-valued amplitude-frequency curve.

F. Expressions for Extreme Cases

In the above, we derived the analytical results for general case. Here, to better understand the nonlinear behavior, we explore several extreme cases. We categorize the cases based on the coupling spring k_{c1} and $\Delta k = k_{11} - k_{21}$. Below, we consider cases of $\Delta k \ll |k_{c1}|$ and $\Delta k \gg |k_{c1}|$ for both positive and negative k_{c1}. Note that no restrictions were made on Δk and $|k_{c1}|$ in solving the nonlinear equation.

1) Positive Coupling Spring ($k_{c1} > 0$) and $k \ll k_{c1}$: In this case, the matrix P reduces to

$$P \approx \frac{1}{\sqrt{2}}\begin{pmatrix} 1 + \frac{\Delta k}{4k_{c1}} & 1 - \frac{\Delta k}{4k_{c1}} \\ -1 + \frac{\Delta k}{4k_{c1}} & 1 + \frac{\Delta k}{4k_{c1}} \end{pmatrix}. \tag{82}$$

Thanks to this simplification, the nonlinearity factors can be explicitly written in terms of mechanical parameters,

$$\mu_1 \approx -\frac{3}{16}\left\{16\epsilon_{c3} + \epsilon_{13}\left(1 + \frac{\Delta k}{k_{c1}}\right) + \epsilon_{23}\left(1 - \frac{\Delta k}{k_{c1}}\right)\right\}, \tag{83}$$

$$\mu_2 \approx -\frac{3}{16}\left\{\epsilon_{13}\left(1 - \frac{\Delta k}{k_{c1}}\right) + \epsilon_{23}\left(1 + \frac{\Delta k}{k_{c1}}\right)\right\}. \tag{84}$$

Note that in the limit of $\Delta k/k_{c1} \to 0$, we get

$$\begin{pmatrix} x_1 \\ x_2 \end{pmatrix} = P\begin{pmatrix} z_1 \\ z_2 \end{pmatrix} \approx \frac{1}{\sqrt{2}}\begin{pmatrix} z_1 + z_2 \\ -z_1 + z_2 \end{pmatrix}. \tag{85}$$

This shows that the second mode represented by z_2 approaches to in-phase mode, which keeps relative distance between x_1 and x_2. The non-existence of ϵ_{c3} term in μ_2 implies that nonlinearity due to the coupling spring can be eliminated in the in-phase mode, as pointed out in [12].

2) Negative Coupling Spring ($k_{c1} < 0$) and $k \ll |k_{c1}|$: Next, we examine the negative coupling spring case ($k_{c1} < 0$). This corresponds to a case when electrostatic attractive force is used for the coupling spring. The matrix P becomes

$$P \approx \frac{1}{\sqrt{2}}\begin{pmatrix} 1 - \frac{\Delta k}{4k_{c1}} & 1 + \frac{\Delta k}{4k_{c1}} \\ 1 + \frac{\Delta k}{4k_{c1}} & -1 + \frac{\Delta k}{4k_{c1}} \end{pmatrix}. \tag{86}$$

This indicates that the first mode z_1 now becomes in-phase mode. The nonlinearity factors are written as

$$\mu_1 \approx -\frac{3}{16}\left\{\epsilon_{13}\left(1 - \frac{\Delta k}{k_{c1}}\right) + \epsilon_{23}\left(1 + \frac{\Delta k}{k_{c1}}\right)\right\}, \tag{87}$$

$$\mu_2 \approx -\frac{3}{16}\left\{16\epsilon_{c3} + \epsilon_{13}\left(1+\frac{\Delta k}{k_{c1}}\right)+\epsilon_{23}\left(1-\frac{\Delta k}{k_{c1}}\right)\right\}. \quad (88)$$

This time, nonlinearity of the coupling spring is eliminated in the first mode, because the first mode is in-phase mode.

3) Positive Coupling Spring ($k_{c1} > 0$) and $k \gg k_{c1}$: As a third case, we consider a case of $k_{c1} > 0$ and $\Delta k \gg k_{c1}$. We assume that Δk is still smaller than k_{11} and k_{21}. In this case, the matrix P reduces to

$$P \approx \begin{pmatrix} 1-\dfrac{k_{c1}^2}{2\Delta k^2} & \dfrac{k_{c1}}{\Delta k} \\ -\dfrac{k_{c1}}{\Delta k} & 1+\dfrac{k_{c1}^2}{2\Delta k^2} \end{pmatrix}. \quad (89)$$

The nonlinearity factors become

$$\mu_1 \approx -\frac{3}{4}\left\{\epsilon_{c3}\left(1+\frac{4k_{c1}}{\Delta k}\right)+\epsilon_{13}\right\}, \quad (90)$$

$$\mu_2 \approx -\frac{3}{4}\left\{\epsilon_{c3}\left(1-\frac{4k_{c1}}{\Delta k}\right)+\epsilon_{23}\right\}. \quad (91)$$

In the limit of $k_{c1}/\Delta k \to 0$, the matrix P becomes diagonal, which suggests that the coupling due to k_{c1} becomes negligible.

4) Negative Coupling Spring ($k_{c1} < 0$) and $k \gg |k_{c1}|$: Finally, we consider a case $k_{c1} < 0$ and $\Delta k \gg |k_{c1}|$. The matrix P for this case is given by

$$P \approx \begin{pmatrix} 1-\dfrac{k_{c1}^2}{2\Delta k^2} & -\dfrac{k_{c1}}{\Delta k} \\ -\dfrac{k_{c1}}{\Delta k} & -1-\dfrac{k_{c1}^2}{2\Delta k^2} \end{pmatrix}. \quad (92)$$

The expressions of nonlinearity factors are the same as the previous case,

$$\mu_1 \approx -\frac{3}{4}\left\{\epsilon_{c3}\left(1+\frac{4k_{c1}}{\Delta k}\right)+\epsilon_{13}\right\}, \quad (93)$$

$$\mu_2 \approx -\frac{3}{4}\left\{\epsilon_{c3}\left(1-\frac{4k_{c1}}{\Delta k}\right)+\epsilon_{23}\right\}. \quad (94)$$

This result implies that if $\epsilon_{13} = \epsilon_{23}$, μ_1 and μ_2 approaches to the same value in the limit of $|k_{c1}|/\Delta k \to 0$.

IV. Analysis of Electrostatic Coupling Spring

Electrostatic force generated by parallel plate electrode is often employed in mode-localized sensors to attain ultra-small coupling spring [2]. But since the electrostatic force is nonlinear, care should be taken about the maximum amplitude. If the nonlinearity is large enough and multiple bifurcation point appear as in Fig. 4 (b), specific type of close-loop system will be required to sustain the peak amplitude [22]. The nonlinearity factors presented above can be used to judge the amount of nonlinearities. To demonstrate this, we numerically analyze a nonlinearity caused by a parallel plate electrode. We also confirm the validity of the theoretical model by comparing the results with FEM simulations.

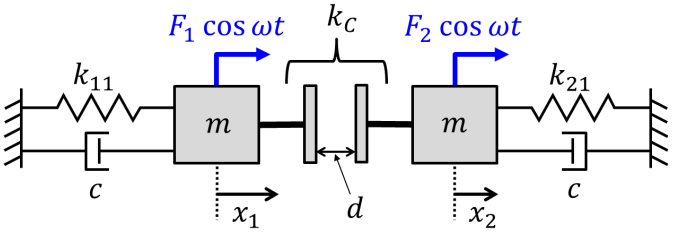

Fig. 5. Weakly coupled resonator with parallel plate electrodes used as a coupling spring. The initial electrode gap is *d*, electrode area is *A*, and voltage *V* is applied between the electrodes.

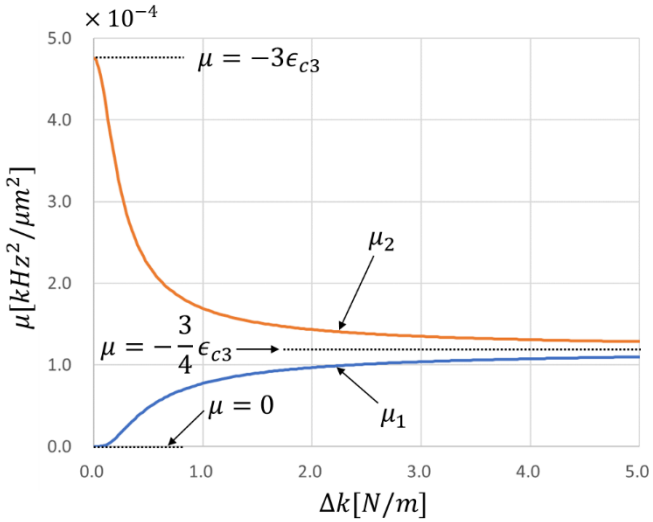

Fig. 6. Nonlinearity factors μ_1 and μ_2 plotted as a function of Δk. The property $\mu_1 \to 0$ at $\Delta k \to 0$ implies elimination of nonlinearity due to the in-phase mode.

A. Coupling Spring by Parallel Plate Electrode

We consider a case when a parallel plate electrode is employed for the coupling spring, as in Fig. 5. We assume that initial gap and area of the electrode are d and A, respectively. In this analysis, we assume that the two outer springs are linear, namely $g_1 = g_2 = 0$. When a voltage V is applied between the electrodes, the electrostatic potential $U(x_1, x_2)$ becomes

$$U(x_1, x_2) = -\frac{\varepsilon_0 A V^2/2}{d-(x_1-x_2)} = -\frac{\varepsilon_0 A V^2}{2d}\sum_{n=0}^{\infty}\left(\frac{x_1-x_2}{d}\right)^n, \quad (95)$$

where ε_0 is the vacuum permittivity; $\varepsilon_0 = 8.854 \times 10^{-12} F/m$. Since the electrostatic force applied to the mass m_i is given by $-\partial U/\partial x_i$, g_c is written as

$$g_c = \sum_{n=2}^{\infty}\epsilon_{cn}(x_1-x_2)^n, \quad (96)$$

where $\epsilon_{cn}(n \geq 2)$ is

$$\epsilon_{cn} = -\frac{(n+1)\varepsilon_0 A V^2}{2md^{n+2}}. \quad (97)$$

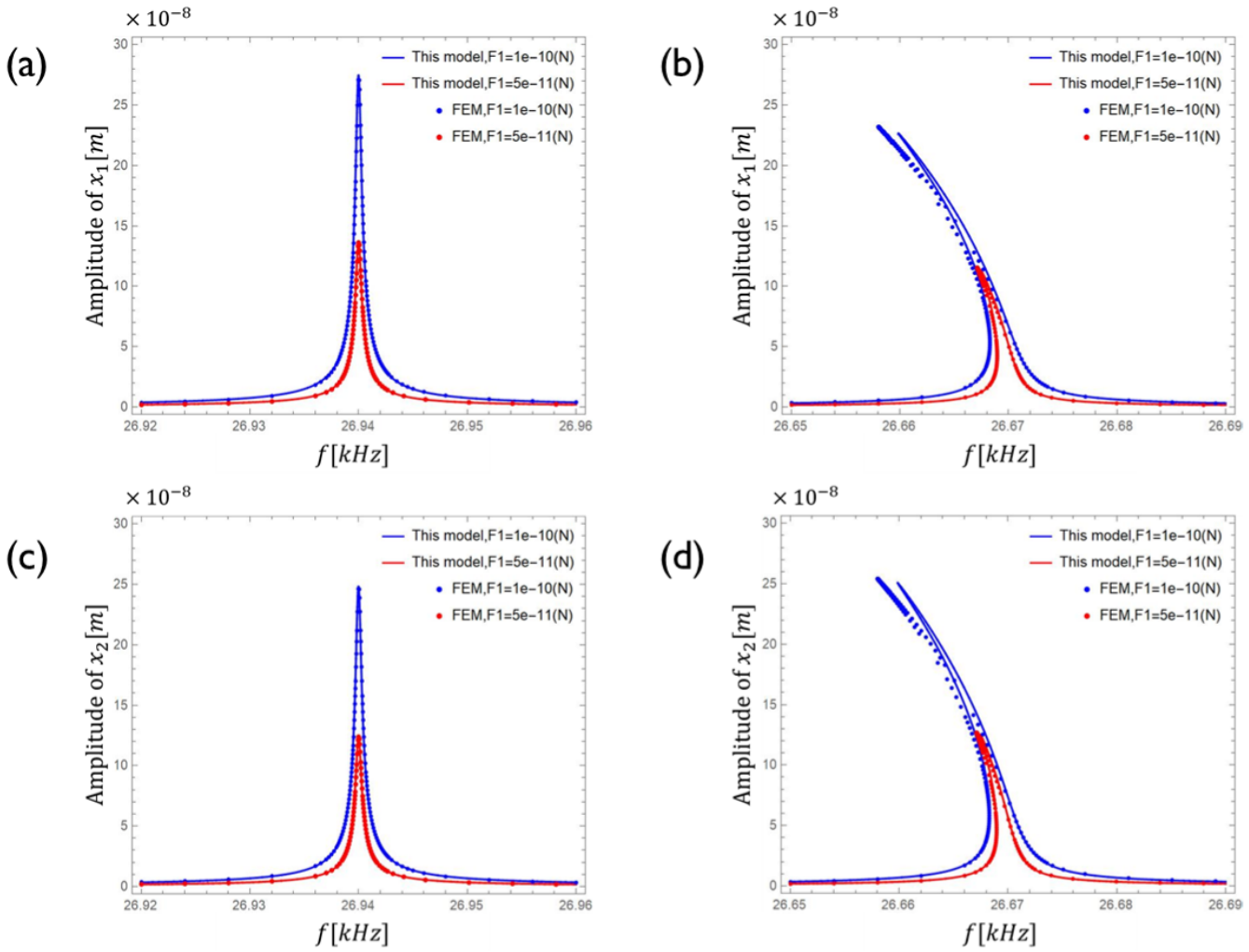

Fig. 7. Amplitude-frequency curves of: (a) x_1 at frequency $\sim f_1$, (b) x_1 at frequency $\sim f_2$, (c) x_2 at frequency $\sim f_1$, (d) x_2 at frequency $\sim f_2$. Solid lines are from the theoretical model and dots are by FEM.

Note that the linear term ($n = 1$) is excluded from g_c and included in k_{c1} of (32) and (33). Explicit form of k_{c1} is

$$k_{c1} = -\frac{\varepsilon_0 A V^2}{d^3}. \tag{98}$$

The minus sign in k_{c1} and ϵ_{cn} implies that these are attractive forces. When applying to our model, we neglect higher order terms of $n \geq 5$.

B. Numerical Analysis of Nonlinearity Factors

To numerically estimate the nonlinear behavior, we assume parameters as in Table I. According to these values, the coupling spring becomes $k_{c1} = -9.84 \times 10^{-2} N/m$. We assume that k_{21} is fixed and k_{11} can be determined from Δk as $k_{11} = k_{21} + \Delta k$.

Then the nonlinearity factors μ_1 and μ_2 can be expressed as a function of Δk, as plotted in Fig. 6. We can see that μ_1 approaches to zero at $\Delta k \to 0$, as predicted by (87). This elimination of nonlinearity is caused by the fact that the first mode approaches to in-phase mode, which keeps the relative distance $x_1 - x_2$ and hence avoids the nonlinearity of the coupling spring. This point is suggested in [12], but our analysis enables to show the occurrence of nonlinearity in quantitative manner. Also, together with (79), we can estimate the force value that brings double bifurcation. We can also see that μ_1 and μ_2 converge to the same value when $\Delta k \gg |k_{c1}|$, as suggested by (93) and (94). Thus, characterization based on the nonlinearity factor is useful to grasp the nonlinear behavior of a system.

TABLE I
PARAMETERS OF ELECTROSTATIC COUPLING SPRING

Symbol	Definition	Value
m	mass	3.5×10^{-10} kg
Q	quality factor	5.0×10^4
k_{21}	spring constant	10 N/m
A	electrode area	3.0×10^{-9} m^2
d	initial electrode gap	3.0×10^{-6} m
V	voltage	10 V

C. Amplitude-Frequency Characteristics

Next, we analyze amplitude-frequency characteristics. To check the accuracy of the model based on the two approximations, we compare the results with FEM simulations. We use parameters in Table I and furthermore, we assume $\Delta k = 0.02N/m$, which suggests $\Delta k \ll |k_{c1}|$. The resonance frequencies of the two modes are $f_1 = 26.94kHz$ and $f_2 = 26.67kHz$. As for the external force, we assume $F_2 = 0$ and consider two cases for F_1; $F_1 = 5.0 \times 10^{-11}N$ and $F_1 = 1.0 \times 10^{-10}N$. Amplitude-frequency curves of the two eigenmodes are described by (73) and (74). Amplitude-frequency curves of position x_1 and x_2 can be obtained by using the matrix P. The results are plotted as solid lines of Fig. 7.

FEM simulations are carried out for the same parameters. To calculate the electrostatic force, we assumed electrode height of 30 μm and width of 100 μm which reproduce the area A of Table I. Coventor's multi-physics simulation tool, *MEMS+*® is employed to simulate the nonlinear characteristics [23]. To reproduce the multi-valued amplitude-frequency curve, Frequency Hysteresis (FH) function of the tool was adopted. FH is a continuation-based algorithms analysis first implemented by Coventor to study pull-in and lift-off effects under a static stimulus [24], [25]. This continuation algorithm applied in the frequency domain allows to compute the multi-valued amplitude-frequency typical behavior of nonlinear resonator such as Duffing. Note that this FEM simulation is calculating the electrostatic force in its complete form. Namely, no truncation is made at finite n of (96). In this sense, the FEM results can be regarded as a reference. The FEM simulation results are plotted as dots in Fig. 7.

Single-valued amplitude-frequency curves shown in Fig. 7 (a) and (c) are reflecting small μ_1 caused by in-phase mode, as suggested by Fig. 6. On the other hand, as in Fig. 7 (b) and (d), multi-valued curves appear for the second mode, as a result of large nonlinearity factor μ_2. Note that the overhanging direction corresponds to the case of spring softening. This is due to negative k_{c1} and ϵ_{cn}. We can also see that the behavior of x_1 and x_2 are similar. This is because every matrix element of P have almost the same magnitude when $\Delta k \ll |k_{c1}|$, as suggested by (86).

Our model matches well with the FEM, especially for the first mode, (a) and (c), and for small force conditions. Slight discrepancy emerges when the force becomes larger in the second mode, (b) and (d). This is likely to be caused by higher order terms of (96), which will become non-negligible when the amplitude becomes closer to the electrode gap. Since the FEM calculates the electrostatic force in full form, we regard that the FEM is reflecting the reality. But our model is sufficient to find the condition of multi-valued amplitude-frequency curve, as can be seen from the curves of small force value. This result also implies that the two approximations employed in the model are legitimate and effective in the analysis of nonlinear coupled resonators.

V. Conclusion

We have solved nonlinear version of WCR based on two approximations; Krylov–Bogoliubov averaging method and approximation based on amplitude-ratio of eigenmodes, and arrived at Duffing-like amplitude-frequency equations. The nonlinearity factors included in the result are found to be useful in characterizing nonlinear behavior of the system, since the factors can be explicitly written by basic parameters. For example, external force value that yields multi-valued amplitude-frequency curve can be known from the nonlinearity factor. Thus, instead of carrying out numerical calculations, we can grasp occurrence and amount of nonlinearity in parameter space. This information can be utilized in selecting sensor system suited for mode-localized sensors. Namely, if the sensor has to be operated in the double bifurcation region, a phase-feedback approach need to be employed [22].

The averaging method we have employed is basically the same as the one of Yang et al [19]. However, our final amplitude-frequency equations are far simpler than theirs. One reason is in the second approximation that uses eigenmode amplitude ratio. Another reason seems to be in the choice of variables. Yang et al have employed variables corresponding to x_1 and $x_1 - x_2$ as the two independent variables. This, however, introduces complication and makes it more difficult to grasp the physical meaning.

This paper has introduced nonlinearity up to fourth order. In principle, however, the averaging method can be applied even if fifth or higher order nonlinearity is included. We would like to leave this analysis as our future work.

The main target of this paper is mode-localized sensors that employ WCR. But nonlinear coupled equation as shown in this paper appears in many fields. Indeed, Yang et al have tried to solve the same nonlinear equation but for different application, i.e., power flow analysis [19]. This means that the methodology and results presented here can be applied for versatile nonlinear systems.

Appendix

A. Explicit Forms of Matrix P and ω_1, ω_2

Matrix P that diagonalize the matrix K in the form of (9) can be obtained by following standard procedure of eigenvalue problem. If we apply the procedure to the matrix K of (35), we obtain

$$P = \begin{pmatrix} p_{11} & p_{12} \\ p_{21} & p_{22} \end{pmatrix} = \begin{pmatrix} \dfrac{1}{\sqrt{1+v_1^2}} & \dfrac{1}{\sqrt{1+v_2^2}} \\ \dfrac{v_1}{\sqrt{1+v_1^2}} & \dfrac{v_2}{\sqrt{1+v_2^2}} \end{pmatrix}, \quad (A1)$$

where

$$v_1 \equiv \frac{k_{11}-k_{21}}{2k_{c1}} - \frac{k_{c1}}{|k_{c1}|}\sqrt{1+\left(\frac{k_{11}-k_{21}}{2k_{c1}}\right)^2}, \quad (A2)$$

$$v_2 \equiv \frac{k_{11}-k_{21}}{2k_{c1}} + \frac{k_{c1}}{|k_{c1}|}\sqrt{1+\left(\frac{k_{11}-k_{21}}{2k_{c1}}\right)^2}. \quad (A3)$$

Note that $v_2 > v_1$ for $k_{c1} > 0$ and $v_1 > v_2$ for $k_{c1} < 0$. The resonant angular frequencies are obtained by taking square

root of the eigenvalues;

$$\omega_1 = \sqrt{\frac{k_{11}+k_{21}+2k_{c1}+\sqrt{(k_{11}-k_{21})^2+4k_{c1}^2}}{2m}}, \quad (A4)$$

$$\omega_2 = \sqrt{\frac{k_{11}+k_{21}+2k_{c1}-\sqrt{(k_{11}-k_{21})^2+4k_{c1}^2}}{2m}}. \quad (A5)$$

B. Explicit Forms of Averaged Results

Here, we show explicit forms of the averaged results, namely, brackets that appear in (54)-(57). In this case, an averaged result $\langle f \rangle$ of a function $f(t)$ is given by

$$\langle f \rangle = \frac{\omega}{2\pi}\int_0^{2\pi/\omega} dt f(t). \quad (B1)$$

Calculation of the brackets are straightforward [18], and the results become as follows;

$$\langle \sigma_1 g_c \cos\theta_1 - \tilde{g}_1 \cos\theta_1 \rangle = a_1^3\Gamma_{30}^1 + a_1^2 a_2 \Gamma_{21}^1 + a_1 a_2^2 \Gamma_{12}^1 + a_2^3\Gamma_{03}^1, \quad (B2)$$

$$\langle \sigma_2 g_c \cos\theta_2 - \tilde{g}_2 \cos\theta_2 \rangle = a_1^3\Gamma_{30}^2 + a_1^2 a_2 \Gamma_{21}^2 + a_1 a_2^2 \Gamma_{12}^2 + a_2^3\Gamma_{03}^2, \quad (B3)$$

$$\langle \sigma_1 g_c \sin\theta_1 - \tilde{g}_1 \sin\theta_1 \rangle = a_1^2 a_2 \Sigma_{21}^1 + a_1 a_2^2 \Sigma_{12}^1 + a_2^3\Sigma_{03}^1, \quad (B4)$$

$$\langle \sigma_2 g_c \sin\theta_2 - \tilde{g}_2 \sin\theta_2 \rangle = a_1^3\Sigma_{30}^2 + a_1^2 a_2 \Sigma_{21}^2 + a_1 a_2^2 \Sigma_{12}^2, \quad (B5)$$

where

$$\Gamma_{30}^1 \equiv \frac{3}{8}\left[\epsilon_{c3}\sigma_1\rho_1^3 - \epsilon_{13}\left(p^{-1}\right)_{11}(p_{11})^3 - \epsilon_{23}\left(p^{-1}\right)_{12}(p_{21})^3\right], \quad (B6)$$

$$\Gamma_{21}^1 \equiv \frac{9}{8}\left[\epsilon_{c3}\sigma_1\rho_1^2\rho_2 - \epsilon_{13}\left(p^{-1}\right)_{11}(p_{11})^2 p_{12} - \epsilon_{23}\left(p^{-1}\right)_{12}(p_{21})^2 p_{22}\right]\cos(\phi_1-\phi_2), \quad (B7)$$

$$\Gamma_{12}^1 \equiv \frac{9}{8}\left[\epsilon_{c3}\sigma_1\rho_1\rho_2^2 - \epsilon_{13}\left(p^{-1}\right)_{11} p_{11}(p_{12})^2 - \epsilon_{23}\left(p^{-1}\right)_{12} p_{21}(p_{22})^2\right]\{\cos 2(\phi_1-\phi_2)+2\}, \quad (B8)$$

$$\Gamma_{03}^1 \equiv \frac{3}{8}\left[\epsilon_{c3}\sigma_1\rho_2^3 - \epsilon_{13}\left(p^{-1}\right)_{11}(p_{12})^3 - \epsilon_{23}\left(p^{-1}\right)_{12}(p_{22})^3\right]\cos(\phi_1-\phi_1), \quad (B9)$$

$$\Gamma_{30}^2 \equiv \frac{3}{8}\left[\epsilon_{c3}\sigma_2\rho_1^3 - \epsilon_{13}\left(p^{-1}\right)_{21}(p_{11})^3 - \epsilon_{23}\left(p^{-1}\right)_{22}(p_{21})^3\right]\cos(\phi_1-\phi_2), \quad (B10)$$

$$\Gamma_{21}^2 \equiv \frac{9}{8}\left[\epsilon_{c3}\sigma_2\rho_1^2\rho_2 - \epsilon_{13}\left(p^{-1}\right)_{21}(p_{11})^2 p_{12} - \epsilon_{23}\left(p^{-1}\right)_{22}(p_{21})^2 p_{22}\right]\{\cos 2(\phi_1-\phi_2)+2\}, \quad (B11)$$

$$\Gamma_{12}^2 \equiv \frac{9}{8}\left[\epsilon_{c3}\sigma_2\rho_1\rho_2^2 - \epsilon_{13}\left(p^{-1}\right)_{21} p_{11}(p_{12})^2 - \epsilon_{23}\left(p^{-1}\right)_{22} p_{21}(p_{22})^2\right]\cos(\phi_1-\phi_2), \quad (B12)$$

$$\Gamma_{03}^2 \equiv \frac{3}{8}\left[\epsilon_{c3}\sigma_2\rho_2^3 - \epsilon_{13}\left(p^{-1}\right)_{21}(p_{12})^3 - \epsilon_{23}\left(p^{-1}\right)_{22}(p_{22})^3\right], \quad (B13)$$

and

$$\Sigma_{21}^1 \equiv \frac{3}{8}\left[\epsilon_{c3}\sigma_1\rho_1^2\rho_2 - \epsilon_{13}\left(p^{-1}\right)_{11}(p_{11})^2 p_{12} - \epsilon_{23}\left(p^{-1}\right)_{12}(p_{21})^2 p_{22}\right]\sin(\phi_1-\phi_2), \quad (B14)$$

$$\Sigma_{12}^1 \equiv \frac{3}{8}\left[\epsilon_{c3}\sigma_1\rho_1\rho_2^2 - \epsilon_{13}\left(p^{-1}\right)_{11} p_{11}(p_{12})^2 - \epsilon_{23}\left(p^{-1}\right)_{12} p_{21}(p_{22})^2\right]\sin 2(\phi_1-\phi_2), \quad (B15)$$

$$\Sigma_{03}^1 \equiv \frac{3}{8}\left[\epsilon_{c3}\sigma_1\rho_2^3 - \epsilon_{13}\left(p^{-1}\right)_{11}(p_{12})^3 - \epsilon_{23}\left(p^{-1}\right)_{12}(p_{22})^3\right]\sin(\phi_1-\phi_2), \quad (B16)$$

$$\Sigma_{30}^2 \equiv -\frac{3}{8}\left[\epsilon_{c3}\sigma_2\rho_1^3 - \epsilon_{13}\left(p^{-1}\right)_{21}(p_{11})^3 - \epsilon_{23}\left(p^{-1}\right)_{22}(p_{21})^3\right]\sin(\phi_1-\phi_2), \quad (B17)$$

$$\Sigma_{21}^2 \equiv -\frac{3}{8}\left[\epsilon_{c3}\sigma_2\rho_1^2\rho_2 - \epsilon_{13}\left(p^{-1}\right)_{21}(p_{11})^2 p_{12} - \epsilon_{23}\left(p^{-1}\right)_{22}(p_{21})^2 p_{22}\right]\sin 2(\phi_1-\phi_2), \quad (B18)$$

$$\Sigma_{12}^2 \equiv -\frac{3}{8}\left[\epsilon_{c3}\sigma_2\rho_1\rho_2^2 - \epsilon_{13}\left(p^{-1}\right)_{21} p_{11}(p_{12})^2 - \epsilon_{23}\left(p^{-1}\right)_{22} p_{21}(p_{22})^2\right]\sin(\phi_1-\phi_2). \quad (B19)$$

REFERENCES

[1] M. Spletzer, A. Raman, A. Q. Wu, X. Xu, and R. Reifenberger, "Ultrasensitive mass sensing using mode localization in coupled microcantilevers," *Appl. Phys. Lett.*, vol. 88, no. 25, 2006, Art. no. 254102.

[2] P. Thiruvenkatanathan, J. Yan, J. Woodhouse, and A. A. Seshia, "Enhancing parametric sensitivity in electrically coupled MEMS resonators," *J. Microelectromech. Syst.*, vol. 18, no. 5, pp. 1077–1086, Oct. 2009.

[3] C. Zhao, M. H. Montaseri, G. S. Wood, S. H. Pu, A. A. Seshia, and M. Kraft, "A review on coupled MEMS resonators for sensing applications utilizing mode localization," *Sens. Actuators A, Phys.*, vol. 249, pp. 93–111, Apr. 2016.

[4] V. Pachkawade, "State-of-the-art in mode-localized MEMS coupled resonant sensors: A comprehensive review," *IEEE Sensors J.*, vol. 21, no. 7, pp. 8751–8779, Apr. 2021.

[5] A. Alassi, M. Benammar, and D. Brett, "Quartz crystal microbalance electronic interfacing systems: A review," *Sensors*, vol. 17, no. 12, p. 2799, Dec. 2017, doi: 10.3390/s17122799.

[6] T. A. Roessig, R. T. Howe, A. P. Pisano, and J. H. Smith, "Surface-micromachined resonant accelerometer," in *Proc. Int. Conf. Solid State Sens. Actuators (TRANSDUCERS)*, vol. 2, Jun. 1997, pp. 859–862.

[7] H. Zhang, B. Li, W. Yuan, M. Kraft, and H. Chang, "An acceleration sensing method based on the mode localization of weakly coupled resonators," *J. Microelectromech. Syst.*, vol. 25, no. 2, pp. 286–296, Apr. 2016.

[8] B. Li, H. Zhang, J. Zhong, and H. Chang, "A mode localization based resonant MEMS tilt sensor with a linear measurement range of 360°," in *Proc. IEEE 29th Int. Conf. Micro Electro Mech. Syst. (MEMS)*, Jan. 2016, pp. 938–941.

[9] B. Peng *et al.*, "A sensitivity tunable accelerometer based on series-parallel electromechanically coupled resonators using mode localization," *J. Microelectromech. Syst.*, vol. 29, no. 1, pp. 3–13, Feb. 2020.

[10] H. Zhang, J. Huang, W. Yuan, and H. Chang, "A high-sensitivity micromechanical electrometer based on mode localization of two degree-of-freedom weakly coupled resonators," *J. Microelectromech. Syst.*, vol. 25, no. 5, pp. 937–946, Oct. 2016.

[11] W. Li, F. Ye, B. Ruan, Y. Hao, and H. Chang, "A mode-localized magnetometer with resolution of 6.9 nT/$\sqrt{\text{Hz}}$ within the range of 100 mT," in *Proc. IEEE Int. Conf. Micro Electro Mech. Syst. (MEMS)*, Jan. 2020, pp. 190–193.

[12] M. Pandit, C. Zhao, A. Mustafazade, G. Sobreviela, and A. A. Seshia, "Nonlinear cancellation in weakly coupled MEMS resonators," in *Proc. Joint Conf. Eur. Freq. Time Forum IEEE Int. Freq. Control Symp. (EFTF/IFC)*, Jul. 2017, pp. 16–19.
[13] M. Manav, A. Srikantha Phani, and E. Cretu, "Mode localized MEMS transducers with voltage-controlled linear coupling," *J. Micromech. Microeng.*, vol. 27, no. 5, 2017, Art. no. 055010.
[14] M. Pandit, C. Zhao, G. Sobreviela, S. Du, X. Zou, and A. Seshia, "Utilizing energy localization in weakly coupled nonlinear resonators for sensing applications," *J. Microelectromech. Syst.*, vol. 28, no. 2, pp. 182–188, Apr. 2019.
[15] H. Zhang *et al.*, "On the sensitivity of mode-localized accelerometers operating in the nonlinear duffing regime," in *Proc. IEEE 34th Int. Conf. Micro Electro Mech. Syst. (MEMS)*, Jan. 2021, pp. 830–833.
[16] C. Zhao, G. Sobreviela, M. Pandit, S. Du, X. Zou, and A. Seshia, "Experimental observation of noise reduction in weakly coupled nonlinear MEMS resonators," *J. Microelectromech. Syst.*, vol. 26, no. 6, pp. 1196–1203, Dec. 2017.
[17] N. M. Krylov and N. N. Bogolyubov, *Introduction to Non-Linear Mechanics*. Princeton, NJ, USA: Princeton Univ. Press, 1947, pp. 8–14.
[18] S. H. Strogatz, *Nonlinear Dynamics and Chaos: With Applications to Physics, Biology, Chemistry, and Engineering*. New York, NY, USA: Perseus Books Publishing L.L.C., 1994, pp. 223–225.
[19] J. Yang, B. Shi, and C. Rudd, "On vibration transmission between interactive oscillators with nonlinear coupling interface," *Int. J. Mech. Sci.*, vol. 137, pp. 238–251, Mar. 2018.
[20] V. Kaajakari, T. Mattila, A. Oja, and H. Seppa, "Nonlinear limits for single-crystal silicon microresonators," *J. Microelectromech. Syst.*, vol. 13, no. 5, pp. 715–724, Oct. 2004.
[21] V. Kaajakari, *Practical MEMS: Design of Microsystems, Accelerometers, Gyroscopes, RF MEMS, Optical MEMS, and Microfluidic Systems*. Las Vegas, NV, USA: Small Gear Publishing, 2009, pp. 419–424.
[22] R. M. C. Mestrom, R. H. B. Fey, and H. Nijmeijer, "On phase feedback for nonlinear MEMS resonators," in *Proc. IEEE Int. Freq. Control Symp. Joint with 21st Eur. Freq. Time Forum*, May 2007, pp. 765–770.
[23] (Sep. 25, 2021). *MEMS+*. [Online]. Available: https://www.coventor.com/products/coventormp/mems-plus/
[24] Z. Zhang, M. Kamon, and L. Daniel, "Continuation-based pull-in and lift-off simulation algorithms for microelectromechanical devices," *J. Microelectromech. Syst.*, vol. 23, no. 5, pp. 1084–1093, Oct. 2014.
[25] M. Kamon *et al.*, "New simulation and experimental methodology for analyzing pull-in and release in MEMS switches," in *Proc. 17th Int. Conf. Solid-State Sens., Actuators Microsyst. (TRANSDUCERS EUROSENSORS)*, Jun. 2013, pp. 2373–2376.

Tamio Ikehashi (Member, IEEE) received the Ph.D. degree in theoretical physics from the University of Tokyo in 1995. In 1995, he joined the Circuit Design Team, Toshiba Corporation, and involved in circuit design of flash memories. He starts research and development of MEMS from 2004. Since 2004, he has been developing various MEMS devices, including RF-MEMS tunable capacitors, pressure sensors, hydrogen sensors, accelerometers, and gyro sensors. Since April 2019, he has been an Associate Professor with Waseda University.

Hideyuki Maekoba received the M.S. degree in physics from the University of Tsukuba, Tsukuba, Ibaraki, Japan, in 1995. He is a Senior Application Engineer at Coventor, where he supports customers in using the CoventorMP® MEMS design product. He is also an expert in the design and modeling of MEMS devices, including RF MEMS, MEMS resonators, and MEMS inertial sensors.

Arnaud Parent received the Ph.D. degree from Paris-Sud University (Paris XI) in 2008. He is a Senior Applications Engineer at Coventor, where he is responsible for technical evaluations, technical customer support, and training for Coventor's MEMS design tools. He previously worked at CEA and ONERA in prototype development of PZT and MEMS gyroscope.